Nat. Hazards Earth Syst. Sci. Discuss., https://doi.org/10.5194/nhess-2018-126
Manuscript under review for journal Nat. Hazards Earth Syst. Sci.
Discussion started: 29 June 2018

Natural Hazards and Earth System Sciences
Discussions

Evaluating critical rainfall conditions for large-scale landslides by detecting event times from seismic records

Hsien-Li Kuo[1], Guan-Wei Lin[1,*], Chi-Wen Chen[2], Hitoshi Saito[3], Ching-Weei Lin[1], Hongey Chen[2,4], Wei-An Chao[5]

[1] Department of Earth Sciences, National Cheng Kung University, No. 1, University Road, Tainan City, 70101, Taiwan
[2] National Science and Technology Center for Disaster Reduction, No. 200, Sec. 3, Beixin Road, Xindin District, New Taipei City, 23143, Taiwan
[3] College of Economics, Kanto Gakuin University, 1-50-1 Mutsuura-higashi, Kanazawa-ku, Yokohama, 236-8501, Japan
[4] Department of Geosciences, National Taiwan University, No.1, Section 4, Roosevelt Road, Taipei, 10617, Taiwan
[5] Department of Civil Engineering, National Chiao Tung University, No. 1001, Daxue Rd., Hsinchu, 30010, Taiwan

Correspondence to: Guan-Wei Lin (gwlin@mail.ncku.edu.tw)

Abstract.

One of the purposes of slope disaster research is to establish an early warning method for rainfall-induced landslides. The insufficient observational records of the past, however, have inhibited the analysis of critical rainfall conditions. This dilemma may be resolved by extracting the times of landslide occurrences from the seismic signals recorded by adjacent seismic stations. In this study, the seismic records of the Broadband Array in Taiwan for Seismology (BATS) were examined to identify the ground motion triggered by large-scale landslides occurring from 2005 to 2014. After the signals from local and teleseismic earthquakes were eliminated, 62 landslide-induced seismic signals were identified. The seismic signals provided the occurrence times of the landslides for assessment of the rainfall conditions, including rainfall intensity (I, mm/h), duration (D, h), and cumulated rainfall (R, mm). Comparison of three common rainfall threshold models (I–D, I–R, and R–D) revealed duration and cumulated rainfall to be the crucial factors in developing a forecast warning model. In addition, a critical volume of water model, $(I\text{-}1.04)\cdot D = 452$ mm, combining statistical and deterministic approaches was established through analysis of rainfall information from the 62 large-scale landslides that occurred.

Key words: large-scale landslide, seismic signal, rainfall threshold, forecast

1. Introduction

In recent years, the frequency of extreme rainfall events has increased globally, as has the number of large-scale natural disasters (Tu and Chou, 2013; Saito et al., 2014). These large-scale natural disasters (e.g., landslides, floods, etc.) cause both huge economic losses and human casualties. In mountainous areas, large-scale landslides (LSLs) can change the landscape and erosion processes as well. Several previous studies have reported that the characteristics of a large-scale landslide may include (1) extremely

Nat. Hazards Earth Syst. Sci. Discuss., https://doi.org/10.5194/nhess-2018-126
Manuscript under review for journal Nat. Hazards Earth Syst. Sci.
Discussion started: 29 June 2018

rapid mass movement, (2) huge landslide volume, and (3) deep-seated excavation into rock formations (Chigira and Kiho, 1994; Lin et al., 2006). However, the discrimination of large-scale and non-large-scale landslides is still indistinct. In practice, the velocity of mass movement and depth of excavation are both difficult to measure, so the landslide area is commonly regarded as an indicator of the scale of a landslide. Although the occurrence frequency of LSLs is lower than that of non-large-scale landslides, known as small-scale landslides (SSLs), LSLs cause rapid changes in the landscape, and the scale of LSL-induced disasters is greater than that of SSLs. Therefore, in this study, a landslide that disturbed an area larger than 0.1 km^2 is considered a large-scale landslide, while one not meeting this criterion is considered a small-scale landslide. It is well known that rainfall plays a significant role in the occurrence of landslides, so thorough understanding of the influences of different rainfall factors is necessary. To reduce losses, the critical rainfall conditions that trigger LSLs must be identified so that a rainfall threshold can be used as a forecast model to execute disaster prevention and mitigation measures.

In past research, it was difficult to estimate the threshold of precipitation convincingly due to the lack of accurate information on the occurrence times of landslides. Recent studies in geophysics (Kanamori et al., 1984; Suriñach et al., 2005; Lin et al., 2010; Ekström and Stark, 2013; Chao et al., 2016; Chao et al., 2017) have suggested that the mass movement of large-scale landslides may generate ground motion. If such ground motion is recorded by seismic stations, the occurrence times of large-scale landslides can be extracted from the records. In one case study, the rainfall that triggered the Xiaolin landslide, a giant landslide in southern Taiwan that disturbed an area of ~2.6 km^2 and resulted in more than 400 deaths in August 2009, was examined. It was found that if the occurrence time of the landslide was unknown, the time error between the conjectured and exact times would be 13 hours, which would result in an erroneous cumulated rainfall measurement of 513.5 mm (Fig. 1). However, with the assistance of seismic records, the time information for estimating critical rainfall can be acquired.

By applying various rainfall factors into statistical analysis, a statistical threshold can be built to explore the critical rainfall conditions of landslide occurrences, such as using rainfall intensity and duration to define rainfall threshold curves (Caine, 1980; Guzzetti et al., 2008; Saito et al., 2010; Chen et al., 2015). Those rainfall thresholds provide valuable information for disaster prevention and mitigation. In this study, we used seismic data recorded by the network of the Broadband Array in Taiwan for Seismology (BATS) (Fig. 2a) and landslide maps generated from satellite images to obtain the exact occurrence times and locations of LSLs. From these, we developed the rainfall threshold for LSLs in Taiwan. Moreover, located at the junction of the Eurasian plate and the Philippine Sea plate, Taiwan has frequent tectonic activity (Ho, 1986; Yu et al., 1997; Willett et al., 2003). Fractural geological conditions coupled with a warm and humid climate, and an average of 3 to 5 typhoon events per year, contribute to the high frequency of slope disasters in mountainous areas in Taiwan (Wang and Ho, 2002; Shieh, 2000; Dadson et al., 2004; Chang

and Chiang, 2009; Chen, 2011). The high coverage of the seismic network and rain gauge stations in Taiwan, coupled with the high occurrence frequency of landslides, make the island a suitable area for examining the use of seismic observations to identify landslide occurrence times and thus the rainfall factors contributing to landslide events.

2. Study Method

2.1 Large-scale landslide mapping

To determine the locations and basic characteristics of LSLs, the landslide areas across the entire island of Taiwan were interpreted using SPOT-4 satellite remote sensing images with a spatial resolution of 10 m in multispectral mode. Images with minimal cloud cover were selected from pre- and post-typhoon and heavy rainfall events. All images were orthorectified to a standard base image and checked manually using fixed visible markers to ensure spatial consistency over time. Figures 2b and 2c show synthetic SPOT images that were used to identify landslides triggered by Typhoon Morakot in 2009. Bare areas are visibly distinguishable in the SPOT images.

The Normalized Difference Vegetation Index (NDVI) was used to conduct a preliminary classification of bare areas (Lin et al., 2004). The exact NDVI thresholds for bare areas differed from one image to another and were determined by tuning the cut-off value based on visible contrasts. After image interpretation, classified areas were clustered based on slope using a digital elevation model with a resolution of 40 m to identify bare areas not associated with landslides (e.g., roads and buildings). The results of the interpretation were compared with a 1:5000 topographic map to exclude areas of interpretation misjudgement, such as fallow farmland or alluvial fans. Landslides induced specifically by a rainstorm event were distinguished by overlaying the pre- and post-event image mosaics. Finally, LSLs and SSLs were distinguished according to the criterion of an affected area of 0.1 km^2. In this study, the types and mechanisms of individual landslides were not investigated, but landslide area was used as the main factor for investigating the rainfall conditions that trigger LSLs.

2.2 Interpretation of ground motions induced by large-scale landslides

The movement of a landsliding mass has several different motion processes, such as sliding, falling, rotation, saltation, rolling and impacting. These complex motion processes act on the ground surface to generate ground motion (Kanamori et al., 1984; Ekström and Stark, 2013). When this ground motion is recorded by adjacent seismic stations, the landslide-related pattern in a spectrogram develops a triangular time/frequency signature in the 1–10 Hz frequency band (Suriñach et al. 2005; Chen et al. 2013). The triangular signature in the spectrogram is the distinctive property that readily distinguishes landslide-induced signals from those of earthquakes and other ambient noise.

The seismic data during typhoons and heavy rainfall events having cumulated rainfall exceeding 500 mm from 2005 to 2014 were collected, and the seismic signals of local earthquakes, regional earthquakes, and teleseismic earthquakes were excluded based on the earthquake catalogues maintained by the United States Geological Survey and the Central Weather Bureau, Taiwan. After the removal of instrument response, mean, and linear trends, a multitaper method (Percival and Walden, 1993; Burtin et al., 2009) was employed for spectral analysis of the continuous seismic records. A 5-min moving window with 50% overlap of the seismic records provided a good spectrogram in the frequency range of 1–10 Hz. Eventually, landslide-related triangular signatures in the spectrograms were manually identified to find the characteristic signals generated by landslides (Fig. 3a, 3b). To reduce the uncertainty caused by the artificial method of identification, only events with very obvious signatures in the spectrograms were used to examine rainfall statistics in this study.

The detection of the occurrence time of landslide-induced ground motion is a substantial key to this study. In seismology, many methods can be used to detect the appearance of the seismic signals of earthquakes, and one of the most widely used methods is the STA/LTA ratio (Allen, 1978). For landslides, the duration of landslide-induced signals usually ranges from tens to hundreds of seconds (Helmstetter and Garambois, 2005; Chen et al., 2013). As compared with the current widely-used rainfall data recorded once per hour, the duration of landslide-induced seismic signals is significantly short. Thus, to avoid misjudgements caused by different signal-detection methods or manual interpretation, this study adopted the time of the maximum amplitude of the envelope of the vertical-component signal recorded in the station closest to the landslide as the occurrence time of the landslide. Considering the transmission speed of seismic waves, a time difference of several seconds to several tens of seconds was negligible with respect to the sampling rate of rainfall records.

To determine which landslides generated ground motion, it was necessary to locate the seismic sources of the signals. However, the arrival times of the *P*- and *S*-waves of landslide-induced ground motion could not be clearly distinguished. As a result, a locating approach proposed by Chen et al. (2013) and Chao et al. (2016) was adopted in this study to locate the landslide-induced signals. The cross-correlation method was used to calculate the correlations between the envelope functions of the seismic signals received by different seismic stations, and subsequently the seismic sources were located with the Monte Carlo method.

Finally, the location results of landslide-induced seismic signals were compared with the exact locations of LSLs interpreted from satellite images (Fig. 3c, 3d). If the locations matched, the occurrence times of the landslides could be obtained, and the time information could be applied to rainfall data analysis.

Nat. Hazards Earth Syst. Sci. Discuss., https://doi.org/10.5194/nhess-2018-126
Manuscript under review for journal Nat. Hazards Earth Syst. Sci.
Discussion started: 29 June 2018

2.3 Analysis methods of rainfall threshold for landslides

In the study, hourly rainfall data were collected from the records of rain gauge stations (Fig. 2a). The major rainfall events analysed in the study were typhoon events. The distribution of precipitation during typhoon events is closely related to the typhoon track and the position of the windward slope. In addition, the density and distribution of rainfall stations in mountainous areas directly affect the results of rainfall threshold analysis. If the landslide location and the selected rainfall station are located in different watersheds, the rainfall information is unlikely to represent the rainfall conditions for the landslide. Therefore, in this study, the selection criteria for a rainfall station were that the rainfall station must be located within the same watershed as the landslide, and at the shortest straight distance from the landslide; moreover, the watershed must be smaller than 100 km^2 in area to ensure that the records at rain gauge stations were sufficient to represent the rainfall at the landslide locations.

In rainfall analysis, the beginning of a rain event is defined as the time point when hourly rainfall exceeds 4 mm, and the rain event ends when the rainfall intensity remains below 4 mm/h for 6 consecutive hours. The critical rainfall condition for a landslide was calculated from the beginning of a rain event to the occurrence time of the landslide. In this way, average rainfall intensity (mm/h), cumulated rainfall (mm), and rainfall duration (h) for each LSL could be used as the factors in the rainfall threshold analysis. In addition to the three factors mentioned above, the daily rainfall for the seven days preceding the rainstorm was considered as antecedent rainfall. The sum of antecedent rainfall and principal event rainfall was regarded as the total effective rainfall (*Rt*). This definition of a rain event has been officially adopted in Taiwan (Jan and Lee, 2004). The use of different definitions of a rain event would result in differences in statistical rainfall conditions, but the statistical criteria used in this study ensured the consistency of data processing in the critical rainfall analysis.

Based on different rainfall factors, three common rainfall threshold analysis methods were used in the study. The first method was the *I-D* method, with the power law curve, $I = aD^{-b}$, where *a* is the scaling parameter (the intercept) of the threshold curve and *b* is the slope (the scaling exponent) (Caine, 1980; Wieczorek, 1987; Keefer et al., 1987). In this study, the *I-D* rainfall threshold curve at 5% exceedance probability was estimated by the method proposed by Brunetti et al. (2010). This threshold was expected to leave 5% of the data points below the threshold line. The second method was the rainfall-based warning model proposed by Jan and Lee (2004), which is based on the *Rt* and *I* product values. With the *Rt-I* method, rainfall intensity and cumulated rainfall were plotted and used to calculate the cumulative probability of the product value of *I* and *Rt* by the Weibull distribution method (Jan and Lee, 2004). The cumulative probability of 5% of *Rt* and *I* product values was taken as the *Rt-I* rainfall threshold. The third method was the *Rt-D* method (Aoki, 1980; Fan et al., 1999). In the *Rt-D* method, the 5% cumulative

Nat. Hazards Earth Syst. Sci. Discuss., https://doi.org/10.5194/nhess-2018-126
Manuscript under review for journal Nat. Hazards Earth Syst. Sci.
Discussion started: 29 June 2018

probability of the product value of *Rt* and *D* by the Weibull distribution method was taken as the *Rt-D* rainfall threshold.

In addition to that of LSLs, the time information of 193 small-scale landslides, such as shallow landslides and debris flows, was collected from the annual reports of debris flows investigated by the Soil and Water Conservation Bureau (SWCB) of Taiwan. This information was applied to the rainfall data analysis and then used to compare the rainfall conditions of the LSLs.

2.4 Critical volume of water mode

Whether a given slope will produce a landslide depends on the balance between the shear strength of the slope material and the downslope component of the gravitational force imposed by the weight of the slope material above a potential slip surface. A critical volume of water model proposed by Keefer et al. (1987) was used in this study to construct a rainfall threshold. The model was derived from existing slope stability theory with some simplifying assumptions. The shear strength of the material at a point within a slope is expressed as:

$$s = c' + (p - u_w)tan\phi' \qquad \text{Eq. (1)}$$

where c' is effective cohesion of material, p is total stress perpendicular to the potential sliding surface, u_w is pore water pressure, and ϕ' is effective friction angle of slope material. The main cause of a slope disaster is the infiltration of rainfall into the slope and accumulation above the impermeable layer, which increases the pore water pressure of the slope material. As the pore water pressure (u_w) increases, the shear strength (s) decreases, eventually leading to slope failure. A critical value of pore water pressure u_{wc} exists in each slope, assuming an infinite slope composed of a non-cohesive sliding surface (c'=0). The pore water pressure threshold can be calculated as:

$$u_{wc} = \mathrm{Z} \cdot \gamma_t[1 - (tan\,\theta \,/\, tan\phi')] \qquad \text{Eq. (2)}$$

where Z is the vertical depth of the sliding surface, γ_t is the unit weight of the slope material, and θ is the slope angle.

As the pore water pressure u_{w} increases to the pore water pressure threshold u_{wc}, a critical volume of water Q_C is retained above the sliding surface until the initiation of slope failure. The Q_C is calculated as:

$$Q_C = (u_{wc}/\gamma_w) \cdot n_{ef} \qquad \text{Eq. (3)}$$

where u_{wc} is the critical value of pore water pressure, γ_w is the unit weight of water, and n_{ef} is the effective porosity, which is the residual porosity of the slope material under free gravity drainage. The drainage rate of a saturated zone is represented by the average value I_0, the unit of which is mm/h. In a heavy rainfall event, the critical quantity of water for causing a slope disaster is defined as:

$$Q_C = (I - I_0) \cdot D \qquad \text{Eq. (4)}$$

Nat. Hazards Earth Syst. Sci. Discuss., https://doi.org/10.5194/nhess-2018-126
Manuscript under review for journal Nat. Hazards Earth Syst. Sci.
Discussion started: 29 June 2018

3. Results

3.1 Topographic features of large-scale landslides

The satellite imagery interpretation showed that, from 2005 to 2014, a total of 686 landslide events with areas greater than 0.1 km^2 occurred in mountainous areas of Taiwan (Fig. 4a). Most of these LSLs had areas of 0.12 to 0.15 km^2, and their slope angles before the landslides occurred were concentrated between 30° and 40° (Fig. 4b). The number of landslides occurring on slope angles exceeding 40° increased after 2010. This increase was most likely due to the fact that during the extremely heavy rainfall of Typhoon Morakot in 2009, more than 2,000 mm precipitated in four days, causing numerous landslides on lower slopes and reducing the stability of the steeper slopes in the following years. The LSLs were primarily concentrated on slopes with elevations ranging from 500 m to 2000 m (Fig. 4c), but the distributions of the highest and lowest elevations of these LSLs showed that the average vertical displacement of these LSLs was greater than 500 m.

The location information of the 193 small-scale landslides investigated by the SWCB was used to obtain the topographic features of the SSLs as well. The distribution of the slope angles of the SSLs was similar to that of the LSLs. However, the distribution of the elevations of the SSLs was quite different from that of the LSLs. Unlike the LSLs, a large portion of the elevations of SSLs was concentrated at about 1000 m. Although the difference in elevation distribution between LSLs and SSLs seems to indicate that the topographic features of LSLs were relatively more widespread than those of SSLs, the situation should be attributed to the limited *in-situ* investigations of the SWCB. Currently, the vast majority of landslides still cannot be investigated in the field.

3.2 The critical rainfall conditions for triggering LSLs

Comparison of the location solutions of seismic signals and the landslide distribution map revealed that the matched LSLs had deviations in distance of 0 to 20 kilometers. In addition to distance, the ground motion traces of the signals were also correlated with the directions of movement of the landslides to reconfirm the matched LSLs. In total, 62 LSLs were paired successfully with seismic record locations (Fig. 2a). These 62 LSLs were distributed in watersheds with high cumulated rainfall during heavy rainfall events. In addition, the 62 LSLs were verified by satellite images from multiple years to guarantee that the shapes and positions were highly credible. Subsequently, the occurrence times of these 62 LSLs were obtained from seismic signals.

The time information was used to implement rainfall analysis. About two-thirds (41) of the LSLs occurred when the total effective rainfall exceeded 1000 mm (Fig. 5). The statistical results of rainfall intensities at the times of LSL occurrences showed that more than half of the LSLs occurred when the rainfall intensity was less than 20 mm/h. Only seven of the LSLs occurred when the rainfall duration was less

Nat. Hazards Earth Syst. Sci. Discuss., https://doi.org/10.5194/nhess-2018-126
Manuscript under review for journal Nat. Hazards Earth Syst. Sci.
Discussion started: 29 June 2018

than 24 hours, and the rainfall durations of these seven events all exceeded 10 hours. The results of single rainfall-factor analysis indicated that the effects of rainfall duration and cumulated rainfall were much more remarkable for LSLs than for SSLs, and that the rainfall intensity at the time of landslide occurrence was not the main factor influencing LSLs. Therefore, the average rainfall intensity was adopted for the following multi-factorial analyses.

4. Rainfall thresholds for LSLs

4.1 Dual rainfall-factor analysis of *I–D*, *I–Rt,* and *Rt–D* thresholds

The single rainfall-factor analysis indicated that there was no significant correlation between landslides and rainfall intensity at the time of LSL occurrences. In the dual rainfall-factor analysis, the *I–D* rainfall threshold was assessed by using the average values of rainfall intensity and rainfall duration. The obtained *I–D* rainfall threshold was $I = 71.9D^{-0.47}$ ($D > 24$ h) (Fig. 6a). We also compared the rainfall information obtained from SSLs that were reported by the SWCB from 2006 to 2014, and the *I–D* rainfall threshold curve for LSLs also fit the lower boundary of the rainfall conditions of SSLs. In addition, the distribution of the rainfall durations indicated that the SSLs were distributed evenly from 3 to 70 hours, while the LSLs were mostly distributed above 20 hours. The rainfall intensity, however, could not be used effectively to distinguish these two kinds of slope disasters. Even under the same rainfall duration, the rainfall intensities of many SSLs were higher than those of LSLs. This result sufficiently demonstrated that rainfall intensity could not be used to distinguish between SSLs and LSLs. Therefore, the *I–D* rainfall threshold may not allow assessment of the landslide scale. It was also found that most of the LSLs with larger areas were concentrated in rainfall durations of more than 50 hours, but the average rainfall intensity was not well-correlated with landslide area. The average rainfall intensity of the SSLs was very high for short durations, but the average duration of the SSLs was much lower than that of LSLs. Therefore, continuous high-intensity rainfall incurs a high likelihood of LSL occurrence.

We also compared the *I–D* rainfall thresholds obtained in the study with those of previous studies that focused on shallow landslides or debris flows. This comparison revealed that the *I–D* threshold curve for LSLs was much higher than the threshold curves for shallow landslides or debris flows.

Based on the analysis of the relationship between total effective rainfall (*Rt*) and rainfall duration (*D*), the product of *Rt* and *D* for LSLs with a cumulative probability of 5% was 12,773 mm·h (Fig. 6b), and the rainfall threshold was also much higher than the 5% cumulative probability of SSLs (487 mm·h). Total effective rainfall differed considerably between LSLs and SSLs. Most SSLs had a total effective rainfall below 500 mm, while only a few SSLs occurred when total effective rainfall exceeded 1000 mm. As a

result of the disparity in the *Rt–D* threshold curves for LSLs and SSLs, it was determined that *Rt–D* analysis could be used effectively to distinguish SSLs from LSLs.

The analysis of the relationship between average rainfall intensity (*I*) and total effective rainfall (*Rt*) revealed that the product value of both factors for 5% cumulative probability was 5,640 mm^2/h (Fig. 6c). The *Rt–I* threshold curve for LSLs was not much higher than that for SSLs (1,541 mm^2/h). Combining the results of the three kinds of dual-factor rainfall threshold analyses revealed that the critical rainfall conditions for SSLs included high average rainfall intensity but relatively low cumulated rainfall, while those for LSLs included long rainfall duration and high effective cumulated rainfall.

The main mechanism of shallow landslides is heavy rainfall along with rapid infiltration, causing soil saturation and a temporary increase in pore-water pressure. However, prolonged rainfall also plays an important role in slow saturation, which in turn influences the groundwater level and soil moisture, and causes LSLs. These facts have been recognized in many studies around the world (Wieczorek and Glade, 2005), but they have been analysed in only a few locations (e.g., a mountainous debris torrent, a shallow landslide event, and an individual rainfall event). Using the regional dataset of landslides and the times information, this study identified the critical rainfall conditions for LSLs and SSLs in Taiwan.

4.2 The critical volume of water model for forecasting LSL

The geological material parameters of the study area (Table 1) were used to calculate the critical volume of water Q_C on the sliding surface, which was found to be 452 mm. The Q_C value was inserted into $Q_C = (I - I_0) \cdot D$ to obtain an I_0 value of 1.04 mm/h, which is more suitable for LSLs than for SSLs, and the threshold curve was rewritten as $(I - 1.04) \cdot D = 452$. The application of this threshold curve to average rainfall intensity and rainfall duration showed that almost all the LSLs could have been forecasted. This application demonstrated a good function as a LSL forecast model (Fig. 6d). In addition, the threshold curve can be used to distinguish LSLs and SSLs clearly. This advantage can prevent or reduce false forecasts. The critical volume of water model combines statistical and deterministic approaches for the assessment of critical rainfall. Therefore, the parameters used to calculate Q_C can be adjusted based on regional geologic and topographic environments within a specific area. The Q_C model illustrates the importance of the cumulative volume of water and rainfall duration to LSLs and takes into account the effects of both infiltration of water and average rainfall intensity. The critical hydrological conditions for LSLs, a long duration and a high amount of cumulated rainfall, can be determined as well.

Although the geological and rainfall conditions in Taiwan and in other countries are not the same, seismic records can be used to obtain the time information of landslide occurrences for rainfall threshold analysis in other countries. For countries with geological and rainfall conditions similar to those of Taiwan (e.g.,

Japan and the Philippines)(Saito and Oguchi, 2005; Yoshimatsu and Abe, 2006; Evans et al., 2007; Yumul et al., 2011), the results of this study may serve as a useful reference for the development of a forecast model for rainfall-triggered landslides.

5. Discussion

5.1 Influence of Typhoon Morakot in 2009 on the rainfall thresholds for LSLs

A previous study has pointed out that because Typhoon Morakot in 2009 was an extreme rainfall event that resulted in 486 large-scale landslides in Taiwan, the surface erosion caused by the typhoon was equivalent to 20 years of accumulated erosion (Chen et al., 2013). Comparison of the data on the rainfall that triggered the LSLs in 2005–2008 with that in 2010–2014 (Fig. 7) revealed that the critical rainfall to trigger a LSL after 2010 was slightly less than it was before 2009. The critical value of *Rt* decreased from 500 mm for the 2005–2008 LSLs to 300 mm for the 2010–2014 LSLs. After Typhoon Morakot, the rainfall threshold for LSLs declined. One possible reason may be that the stability of potential slopes was affected by the excessive rainfall of Typhoon Morakot, which led to a decrease in the rainfall threshold after 2009. The other possible reason may be that some of the SSLs that occurred in 2005–2009 disturbed adjacent slopes, leaving old landslides prone to expansion. However, due to the limited amount of LSL rainfall data, the slight difference in rainfall thresholds is still difficult to view as solid evidence in support of the decline in critical rainfall conditions for triggering LSLs.

5.2 Rainfall thresholds for different rock types

Among the 62 LSLs, 23 LSLs were located in slate, 23 LSLs occurred in schist, 11 LSLs occurred in interbedded sedimentary rocks, and 5 LSLs were located in meta-sandstone. From the relationship between total effective rainfall and rainfall duration (Fig. 8), it was found that the critical *Rt* for schist was the lowest. Schist is a kind of foliated metamorphic rock that is prone to abundant crack propagation along with sudden loss of cohesion. The cracks in the rock mass become both a path for water infiltration and the interface of rock mass separation or collapse. By contrast, the critical value of *Rt* for metamorphic sandstone is relatively higher. LSLs on meta-sandstone occurred only when *Rt* exceeded 500 mm. In comparison, schist LSLs occurred when *Rt* was lower than 500 mm. In general, meta-sandstone has a compact texture, which leads to high strength.

The main path of water infiltration into the ground is usually dense cracks generated in rocks. However, the differences in the critical values of *Rt* for LSLs in different rock types are limited (Fig. 8). In addition, the rainfall data that could be used for developing rainfall thresholds for LSLs in each rock type are insufficient. Although we would like to discuss the influences of rock types on the occurrence of LSLs,

it is obvious from the current data that the differences in critical rainfall between different rock types are not significant.

5.3 Limitation of seismic detection for LSLs

The number of LSLs detected from seismic records, 62, comprised only nine percent of the total LSLs in 2005–2014 in Taiwan. This low percentage indicates that the vast majority of LSLs were not well identified from seismic records. If this limitation can be surmounted, more time information on LSL occurrences can be used to develop rainfall thresholds. The average interstation spacing of the Broadband Array in Taiwan for Seismology is around 30 km. A higher density of seismic stations would improve the detection function. In addition, to determine the limitation of LSL detection distance as a function of LSL disturbed area, the most distant seismic station where LSL signals were visible was selected. Some previous studies have applied similar approaches to probe the detection limit (Dammeier et al., 2011; Chen et al., 2013). The relationship between the maximum distance of detection and the LSL-disturbed area shows a limitation of the detection distance due to the LSL's magnitude (Fig. 9). As a LSL's area increases, the maximum distance between the LSL location and seismic detection increases. An upper detection limit can be described by

$$\log(distance) = 0.5069 * \log(area) - 1.3443 \qquad \text{Eq. (5)}$$

For a given LSL, if a station is located below the upper detection limit, the seismic signal should be detectable. However, not all the stations located in detectable regions recorded clear LSL-induced seismic signals. One of the possible reasons is that the environmental background noise affected the signal to noise ratio of the seismic records during heavy rainfall events. Therefore, the detection limit may also depend on the signal quality at each station.

6. Conclusion

In this study, seismic signals recorded by a broadband seismic network were used to determine the exact times of occurrence of large-scale landslides (LSLs), and the rainfall threshold for LSLs was assessed statistically based on the time information. Based on the rainfall information of 62 LSLs that occurred from 2005 to 2014 in Taiwan, the rainfall conditions for triggering LSLs include total effective rainfall of more than 1000 mm and rainfall duration of more than 24 hours. After the rainfall thresholds were analysed by the *I-D*, *Rt-D*, and *Rt-I* methods, the rainfall thresholds based on different dual factors for triggering LSLs were obtained. Furthermore, a critical water model combining statistical and deterministic approaches was developed to figure out a three-factor threshold for LSLs. The rainfall information and geologic/topographic parameters finally were applied to obtain the threshold curve, $(I\text{-}1.04)\cdot D = 452$, where average rainfall intensity I is in mm/h and rainfall duration D is in h. This new critical model can be used to improve the forecasting of LSLs and will not lead to confusion between SSLs and LSLs. The influences of extreme rainstorm events and rock types on the rainfall threshold were

also investigated. However, the changes in the rainfall thresholds for LSLs either before or after an extreme event or in different rock types were not notable.

Acknowledgement

The authors gratefully acknowledged the financial support of the Ministry of Science and Technology of Taiwan and the Soil and Water Conservation Bureau, Council of Agriculture, Executive Yuan of Taiwan. The source of all seismic and rainfall information included in this paper was the Institute of Earth Sciences, Academia Sinica of Taiwan, and the Seismology Center, Central Weather Bureau (CWB), Taiwan.

References

Allen, R. V.: Automatic earthquake recognition and timing from single traces, Bulletin of the Seismological Society of America, 68(5), 1521-1532, 1978.

Aoki, S.: Critical rainfall triggering debris-flow disaster, National Research Institute for Earth Science and Disaster Prevention, 38, 22-26, (in Japanese), 1980.

Brunetti, M. T., Peruccacci, S., Rossi, M., Luciani, S., Valigi, D., and Guzzetti, F.: Rainfall thresholds for the possible occurrence of landslides in Italy, Natural Hazards and Earth System Sciences, 10, 447-458, 2010.

Burtin, A., Bollinger, L., Cattin, R., Vergne, J., and Nabelek, J. L.: Spatiotemporal sequence of Himalayan debris flow from analysis of high-frequency seismic noise, Journal of Geophysical Research, 114, F4, 2009.

Caine, N.: The rainfall intensity: duration control of shallow landslides and debris flows, Geografiska Annaler. Series A. Physical Geography, 62, 23-27, 1980.

Chang, K. and Chiang, S.: An integrated model for predicting rainfall-induced landslides, Geomorphology, 105, 366–373, 2009.

Chao, W. A., Zhao, L., Chen, S. C., Wu, Y. M., Chen, C. H. and Huang, H. H.: Seismology-based early identification of dam-formation landquake events, Scientific reports, 6, 19259, 2016.

Chen, C. H., Chao, W. A., Wu, Y. M., Zhao, L., Chen, Y. G., Ho, W. Y., Lin, T. L., Kuo, K. H., and Chang, J. M.: A seismological study of landquakes using a real-time broad-band seismic network, Geophysical Journal International, 194(2), 885-898, 2013.

Chen, C. W., Saito, H., and Oguchi, T.: Rainfall intensity–duration conditions for mass movements in Taiwan, Progress in Earth and Planetary Science, 2, 1-13, 2015.

Chen, J. C.: Variability of impact of earthquake on debris-flow triggering conditions: case study of Chen-Yu-Lan watershed, Taiwan, Environmental Earth Sciences, 64(7), 1787–1794, 2011.

Chen, Y. C., Chang, K. T., Chiu, Y. J., Lau, S. M., and Lee, H. Y.: Quantifying rainfall controls on catchment-scale landslide erosion in Taiwan, Earth Surface Processes and Landforms, 38, 372-382, 2013.

Chigira, M., and Kiho, K.: Deep-seated rockslide-avalanches preceded by mass rock creep of sedimentary rocks in the Akaishi Mountains, central Japan, Engineering Geology, 38(3-4), 221-230, 1994.

Dadson, S. J., Hovius, N., Chen, H., Dade, W. B., Lin, J. C., Hsu, M. L., Lin, C. W., Horng, M. J., Chen, T. C., Milliman, J., and Stark, C. P.: Earthquake triggered increase in sediment delivery from an active mountain belt, Geology, 32, 733–736, 2004.

Dammeier, F., Moore, J. R., Haslinger, F., and Loew, S.: Characterization of alpine rockslides using statistical analysis of seismic signals, Journal of Geophysical Research, 116, F04024, 2011.

Ekström, G., and Stark, C. P.: Simple scaling of catastrophic landslide dynamics, Science, 339, 1416-1419, 2013.

Evans, S. G., Guthrie, R. H., Roberts, N. J., and Bishop, N. F.: The disastrous 17 February 2006 rockslide-debris avalanche on Leyte Island, Philippines: a catastrophic landslide in tropical mountain terrain, Natural Hazards and Earth System Science, 7(1), 89-101, 2007.

Fan, J. C., Wu, M. F., and Peng, G. T.: The Critical Rainfall Line of Debris Flow Occurrence at Feng-Chiou, Sino-Geotechnics, 74, 39-46, 1999.

Guzzetti, F., Peruccacci, S., Rossi, M., and Stark, C. P.: Rainfall thresholds for the initiation of landslides in central and southern Europe, Meteorology and atmospheric physics, 98(3), 239-267, 2007.

Guzzetti, F., Peruccacci, S., Rossi, M., and Stark, C. P.: The rainfall intensity–duration control of shallow landslides and debris flows: an update, Landslides, 5(1), 3-17, 2008.

Handin, J., and Hager Jr, R. V.: Experimental deformation of sedimentary rocks under confining pressure: Tests at room temperature on dry samples, AAPG Bulletin, 41(1), 1-50, 1957.

Handin, J., Hager Jr, R. V., Friedman, M., and Feather, J. N.: Experimental deformation of sedimentary rocks under confining pressure: pore pressure tests, AAPG Bulletin, 47(5), 717-755, 1963.

Helmstetter, A., and Garambois, S.: Seismic monitoring of Séchilienne rockslide (French Alps): Analysis of seismic signals and their correlation with rainfalls, Journal of Geophysical Research: Earth Surface, 115(F3), 2010.

Ho, C. S.: A synthesis of the geologic evolution of Taiwan, Tectonophysics, 125, 1–16, 1986.

Jan, C. D., and Lee, M. H.: A Debris-Flow Rainfall-Based Warning Model, Journal of Chinese Soil and Water Conservation, 35, 275-285, 2004.

Jan, C. D., and Chen, C. L.: Debris flows caused by Typhoon Herb in Taiwan, In Debris-Flow Hazards and Related Phenomena, Springer Berlin Heidelberg, 539-563, 2005.

Kanamori, H., Given, J. W., and Lay, T.: Analysis of seismic body waves excited by the Mount St. Helens eruption of May 18, 1980, Journal of Geophysical Research: Solid Earth, 89, 1856-1866, 1984.

Keefer, D. K., Wilson, R. C., Mark, R. K., Brabb, E. E., Brown, W. M., Ellen, S. D., and Zatkin, R. S.: Real-time landslide warning during heavy rainfall, Science, 238, 921-925, 1987.

Lin, C. W., Liu, S. H., Lee, S. Y., and Liu, C. C.: Impacts of the Chi-Chi earthquake on subsequent rainfall-induced landslides in central Taiwan, Engineering Geology, 86(2), 87-101, 2006.

Lin, C. W., Shieh, C. L., Yuan, B. D., Shieh, Y. C., Liu, S. H. and Lee, S. Y.: Impact of Chi-Chi earthquake on the occurrence of landslides and debris flows: Example from the Chenyulan River watershed, Nantou, Taiwan, Engineering geology, 71, 49–61, 2004.

Lin, C., Kumagai, H., Ando, M., and Shin, T.: Detection of landslides and submarine slumps using broadband seismic networks. Geophysical Research Letters, 37, L22309, 1-5, 2010.

Percival, D. B., and Walden, A. T.: Spectral analysis for physical applications: Multitaper and conventional univariate techniques, Cambridge Univ. Press, Cambridge, U. K, 1993.

Saito, H., Nakayama, D., and Matsuyama, H.: Relationship between the initiation of a shallow landslide and rainfall intensity—duration thresholds in Japan, Geomorphology, 118(1), 167-175, 2010.

Saito, H., Korup, O., Uchida, T., Hayashi, S., and Oguchi, T.: Rainfall conditions, typhoon frequency, and contemporary landslide erosion in Japan, Geology, 42(11), 999-1002, 2014.

Saito, K., and Oguchi, T.: Slope of alluvial fans in humid regions of Japan, Taiwan and the Philippines, Geomorphology, 70(1), 147-162, 2005.

Shieh, S. L.: User's Guide for Typhoon Forecasting in the Taiwan Area (VIII), Central Weather Bureau, Taipei Aman, 2000.

Suriñach, E., Vilajosana, I., Khazaradze, G., Biescas, B., Furdada, G., and Vilaplana, J.: Seismic detection and characterization of landslides and other mass movements, Natural Hazards and Earth System Science, 5, 791-798, 2005.

Tu, J. Y., and Chou, C.: Changes in precipitation frequency and intensity in the vicinity of Taiwan: typhoon versus non-typhoon events, Environmental Research Letters, 8, 1-7, 2013.

Wang, B., and Ho, L.: Rainy season of the Asian-Pacific summer monsoon, J. Climate, 15, 386–398, 2002.

West, T. R.: Geology applied to engineering. Prentice Hall, Inc., Simon/Schuster Company, Englewood Cliffs, New Jersey, 07632, 541, 1995.

Wieczorek, G. F.: Effect of rainfall intensity and duration on debris flows in central Santa Cruz Mountains, California, Reviews in Engineering Geology, 7, 93-104, 1987.

Wieczorek, G., and Glade, T.: Climatic Factors Influencing Occurrence of Debris Flows. In: Jakob, M. and Hungr, O., Eds., Debris-Flow Hazards and Related Phenomena, Springer, Berlin, 325-362, 2005.

Willett, S. D., Fisher, D., Fuller, C., Yeh, E.C., and Lu, C. Y.: Erosion rates and orogenic wedge kinematics in Taiwan inferred from apatite fission track thermochronometry, Geology, 31, 945–948, 2003.

Yoshimatsu, H., and Abe, S.: A review of landslide hazards in Japan and assessment of their susceptibility using an analytical hierarchic process (AHP) method, Landslides, 3(2), 149-158, 2006.

Yu, S. B., Chen, H. Y., and Kuo, L. C.: Velocity field of GPS stations in the Taiwan area, Tectonophysics, 274, 41–59, 1997.

Yumul, G. P., Cruz, N. A., Servando, N. T., and Dimalanta, C. B.: Extreme weather events and related disasters in the Philippines, 2004–08: a sign of what climate change will mean, Disasters, 35(2), 362-382, 2011.

Nat. Hazards Earth Syst. Sci. Discuss., https://doi.org/10.5194/nhess-2018-126
Manuscript under review for journal Nat. Hazards Earth Syst. Sci.
Discussion started: 29 June 2018

Natural Hazards and Earth System Sciences
Discussions

Table 1. Parameters for calculating critical volume of water Q_C

vertical depth of sliding surface, Z	10 m
unit weight of slope material, γ_t	2.65 t/m^2
average slope angle, θ	32 °
effective friction angle, ϕ'	37 °
effective porosity, n_{ef}	0.1

*The vertical depth of a sliding surface of 10 m is adopted according to the definition of LSLs. The average slope angle is the average slope degree of the 62 detected LSLs. The ϕ' value is quoted from Handin et al. (1957, 1963). The n_{ef} value is a median value according to experimental data reported by West (1995).

Nat. Hazards Earth Syst. Sci. Discuss., https://doi.org/10.5194/nhess-2018-126
Manuscript under review for journal Nat. Hazards Earth Syst. Sci.
Discussion started: 29 June 2018

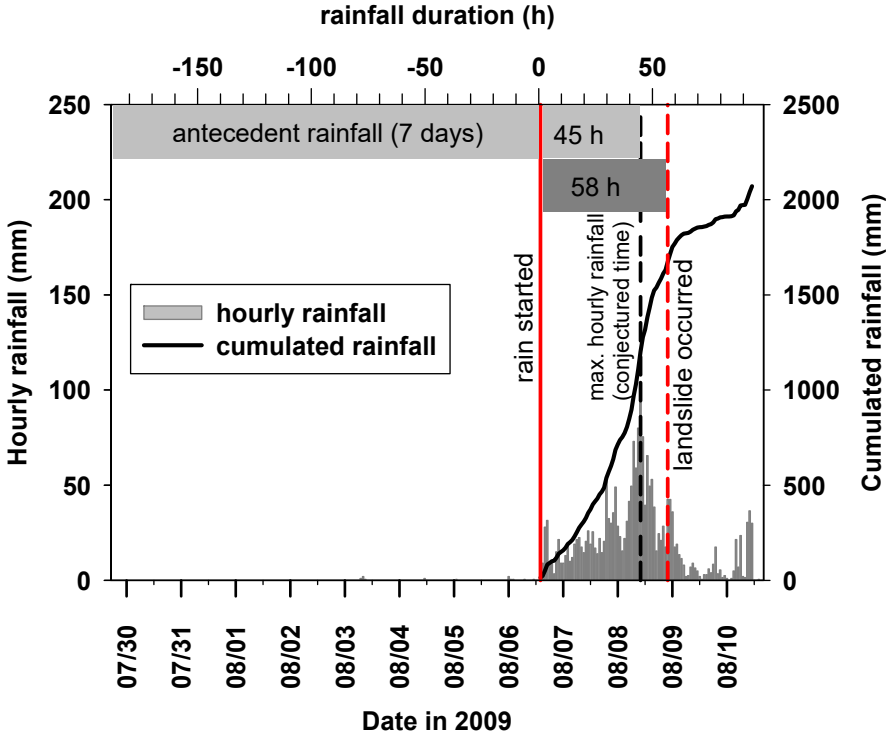

Fig. 1. Time series of hourly rainfall and cumulative rainfall from July 29 to August 10, 2009. Rainfall data were collected from the CWB C0V250 rainfall gauge station, which is 12 km from the Xiaolin landslide. The Xiaolin landslide occurred at UTC 22:16 on August 8, 2009. The rainfall event induced by Typhoon Morakot in 2009 started at UTC 14:00 on August 6, when hourly rainfall exceeded 4 mm. The maximum hourly rainfall was at UTC 10:00 on August 8. In general, if the exact time of landslide occurrence cannot be investigated, the time point with the maximum hourly rainfall will be conjectured as the occurrence time of the landslide.

Nat. Hazards Earth Syst. Sci. Discuss., https://doi.org/10.5194/nhess-2018-126
Manuscript under review for journal Nat. Hazards Earth Syst. Sci.
Discussion started: 29 June 2018

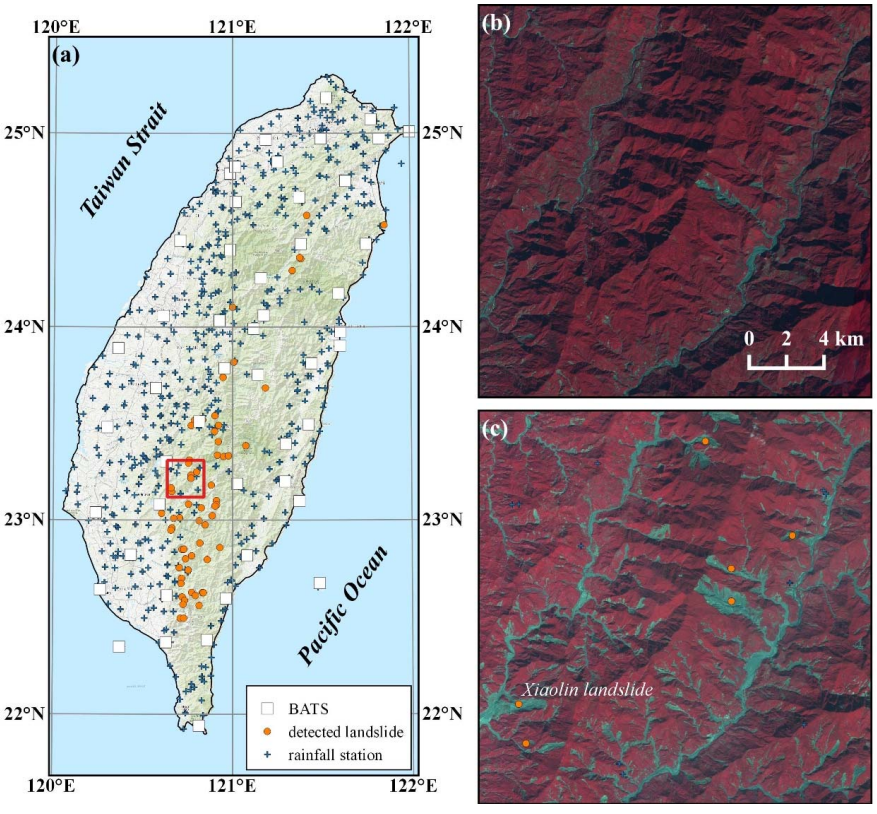

Fig. 2. Comparison of satellite images pre- and post-Typhoon Morakot. (a) Overview map of Taiwan and distribution of rainfall gauge stations. The red frame denotes the areas displayed in (b) and (c). (b) SPOT image taken between January and June 2009. (c) SPOT image taken between September and December 2009.

Nat. Hazards Earth Syst. Sci. Discuss., https://doi.org/10.5194/nhess-2018-126
Manuscript under review for journal Nat. Hazards Earth Syst. Sci.
Discussion started: 29 June 2018

Natural Hazards and Earth System Sciences
Discussions

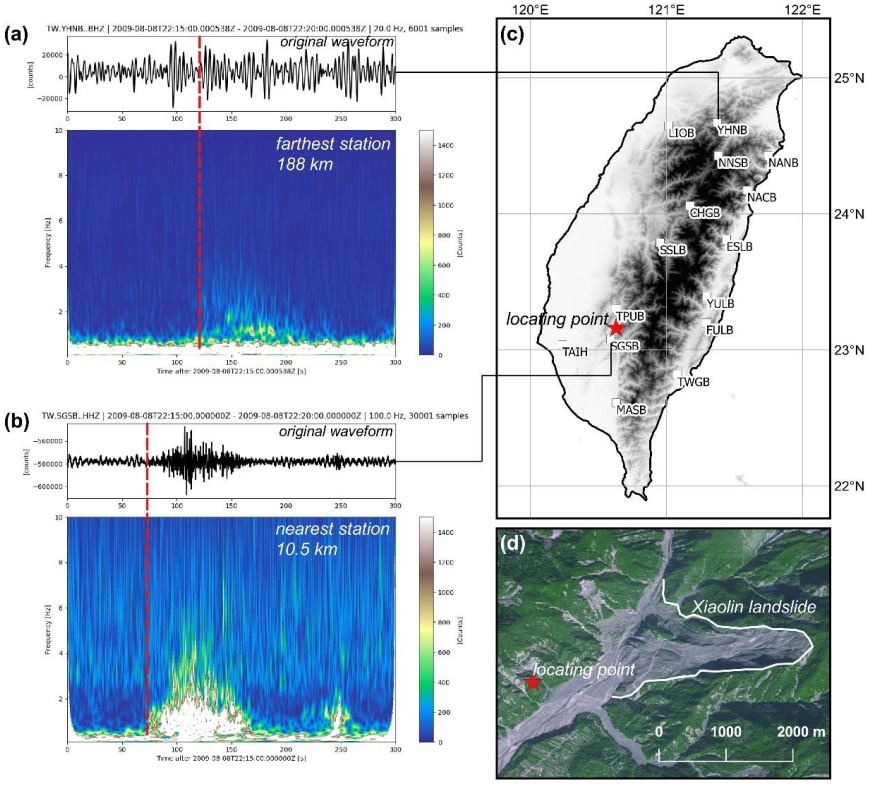

Fig. 3. Characteristic triangle signature visible in a spectrogram within a time window starting at UTC 22:15 and ending at UTC 22:20 on August 8, 2009. (a) Original waveform and spectrogram of the vertical component at station YHNB. (b) Original waveform and spectrogram of the vertical component at station MASB. (c) Distribution of 15 detections of ground motion induced by the Xiaolin landslide and the location result. (d) The location point and the location of the Xiaolin landslide. The location error between the location result and the landslide site is about 1.5 km.

Nat. Hazards Earth Syst. Sci. Discuss., https://doi.org/10.5194/nhess-2018-126
Manuscript under review for journal Nat. Hazards Earth Syst. Sci.
Discussion started: 29 June 2018

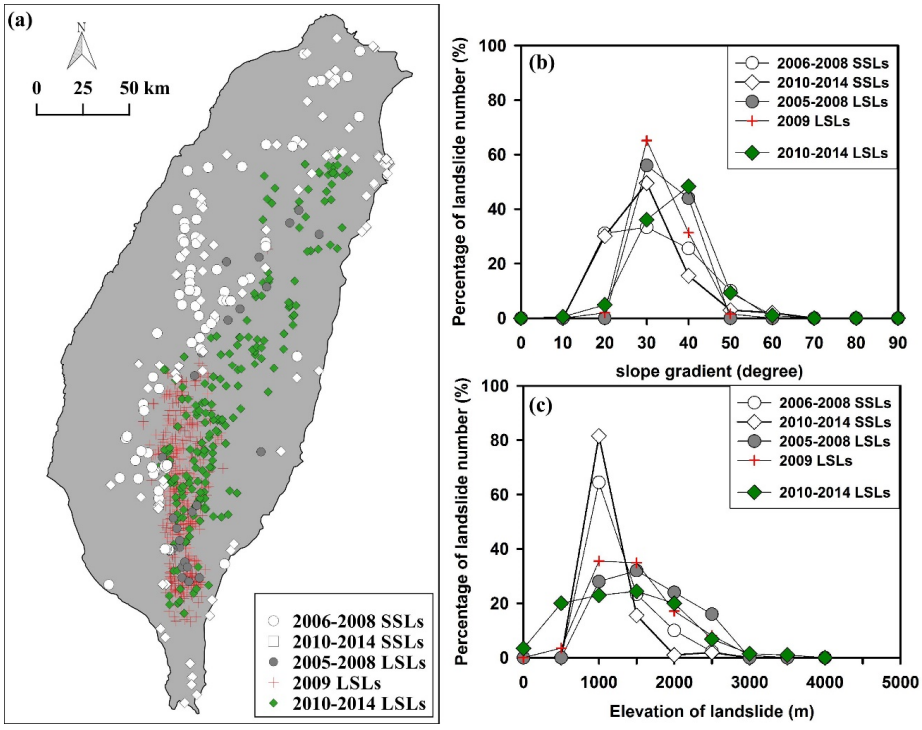

Fig. 4. (a) Distribution map of LSLs from 2005 to 2014 and SSLs from 2006 to 2014. (b) The numerical distribution of slope gradients of LSLs and SSLs, presented in percentages. (c) The numerical distribution of elevations of LSLs and SSLs, presented in percentages.

Nat. Hazards Earth Syst. Sci. Discuss., https://doi.org/10.5194/nhess-2018-126
Manuscript under review for journal Nat. Hazards Earth Syst. Sci.
Discussion started: 29 June 2018

Natural Hazards and Earth System Sciences
Discussions

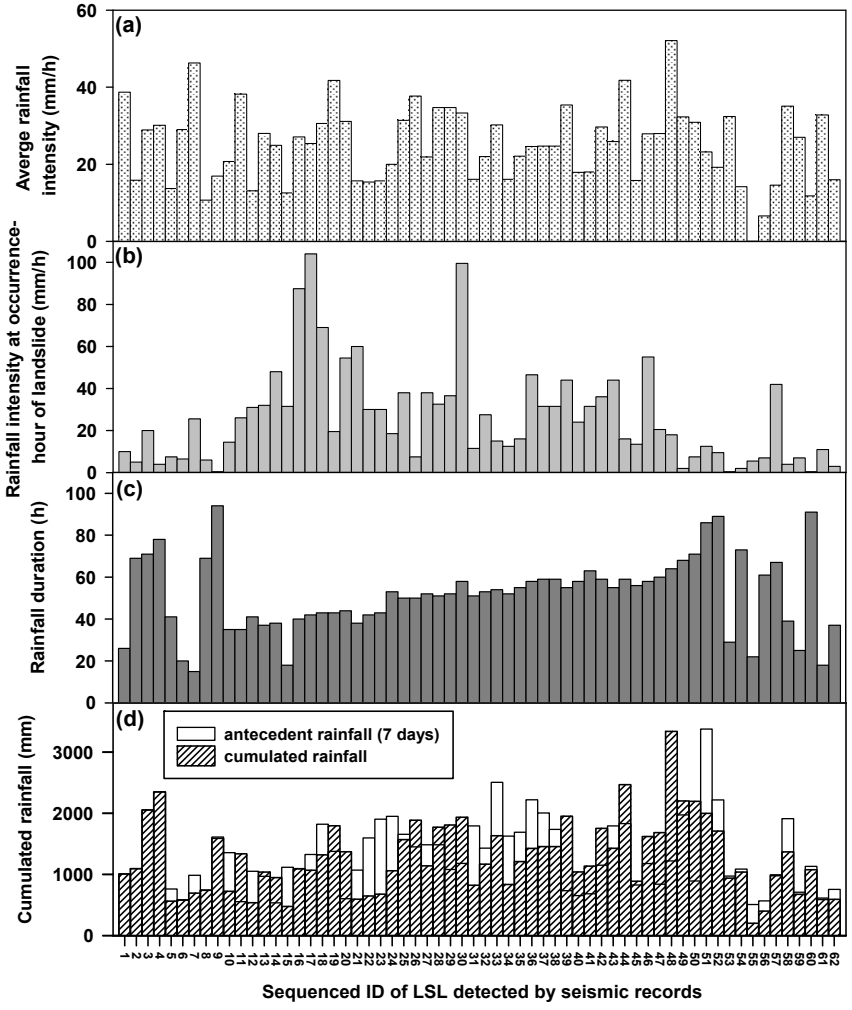

Fig. 5. Single-factor rainfall analysis. Each LSL is assigned an ID number in the figure. The ID numbers of LSLs are displayed in chronological order. ID 1–4 are the LSLs occurring in 2005; ID 5 is a LSL occurring in 2006; ID 6–9 are the LSLs occurring in 2008; ID 10–52 are the LSLs occurring in 2009; ID 53 is a LSL occurring in 2010; ID 54–56 are the LSLs occurring in 2011; ID 57–60 are the LSLs occurring in 2012; ID 61–62 are the LSLs occurring in 2013. No LSLs occurring in 2007 or 2014 were successfully paired with the seismic signal results. Most LSLs occurred when rainfall duration exceeded 24 hours, cumulative rainfall exceeded 1000 mm, and rainfall intensity was less than 20 mm/h.

Nat. Hazards Earth Syst. Sci. Discuss., https://doi.org/10.5194/nhess-2018-126
Manuscript under review for journal Nat. Hazards Earth Syst. Sci.
Discussion started: 29 June 2018

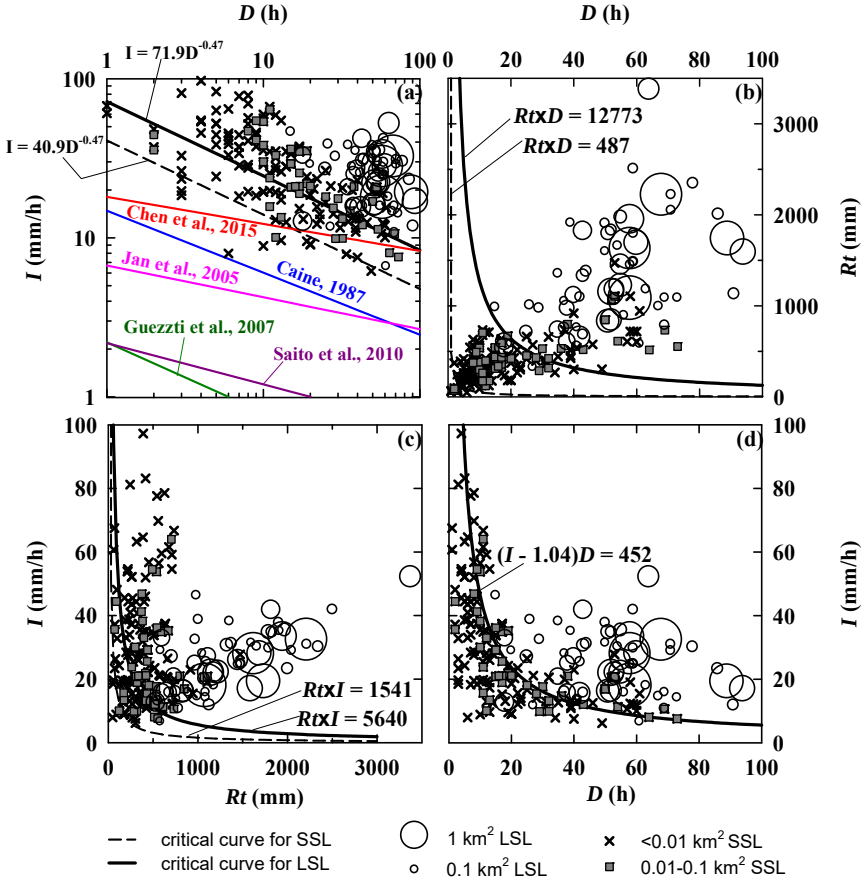

Fig. 6. (a) *I-D* rainfall threshold. (b) *Rt-D* method rainfall threshold. (c) *Rt-I* method rainfall threshold. (d) Threshold of the critical volume of water model.

Nat. Hazards Earth Syst. Sci. Discuss., https://doi.org/10.5194/nhess-2018-126
Manuscript under review for journal Nat. Hazards Earth Syst. Sci.
Discussion started: 29 June 2018

Natural Hazards and Earth System Sciences
Discussions

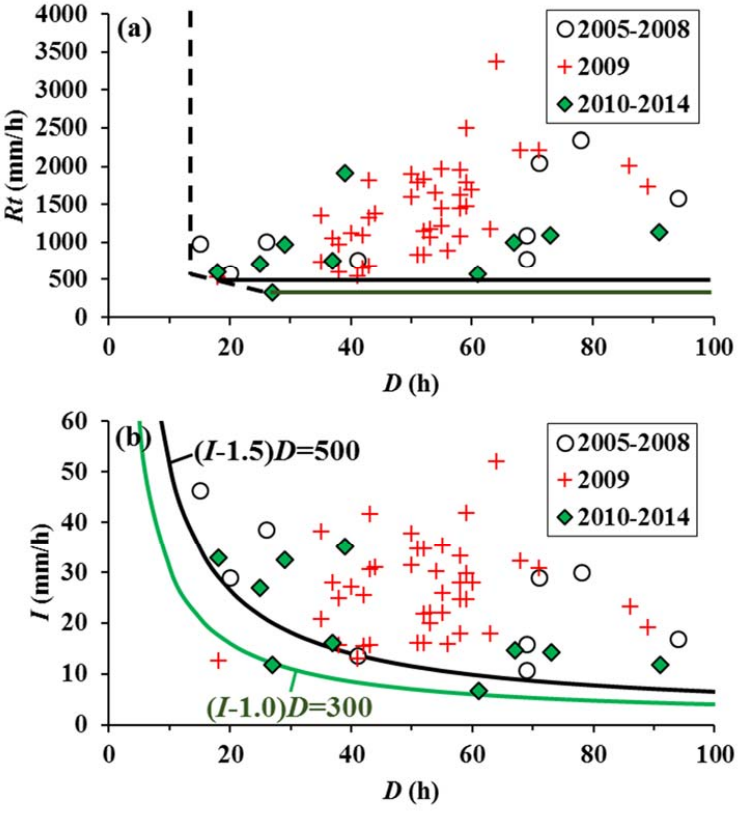

Fig. 7. (a) Variation of rainfall duration and cumulated rainfall. (b) Comparison of critical volume of water thresholds before and after 2009. The black solid line indicates the lower boundary of the 2005–2008 data. The green line indicates the lower boundary of the 2010–2014 data.

Nat. Hazards Earth Syst. Sci. Discuss., https://doi.org/10.5194/nhess-2018-126
Manuscript under review for journal Nat. Hazards Earth Syst. Sci.
Discussion started: 29 June 2018

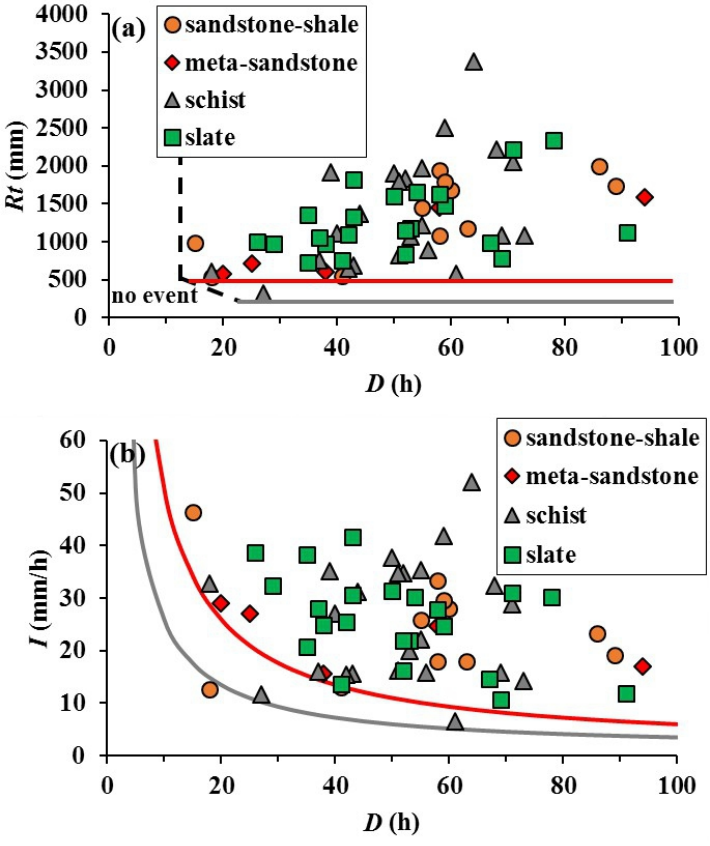

Fig. 8. Comparison of critical thresholds for different rock types. The grey line indicates the lower boundary of LSLs occurring on schist. The red line indicates the lower boundary of LSLs occurring on meta-sandstone.

Nat. Hazards Earth Syst. Sci. Discuss., https://doi.org/10.5194/nhess-2018-126
Manuscript under review for journal Nat. Hazards Earth Syst. Sci.
Discussion started: 29 June 2018

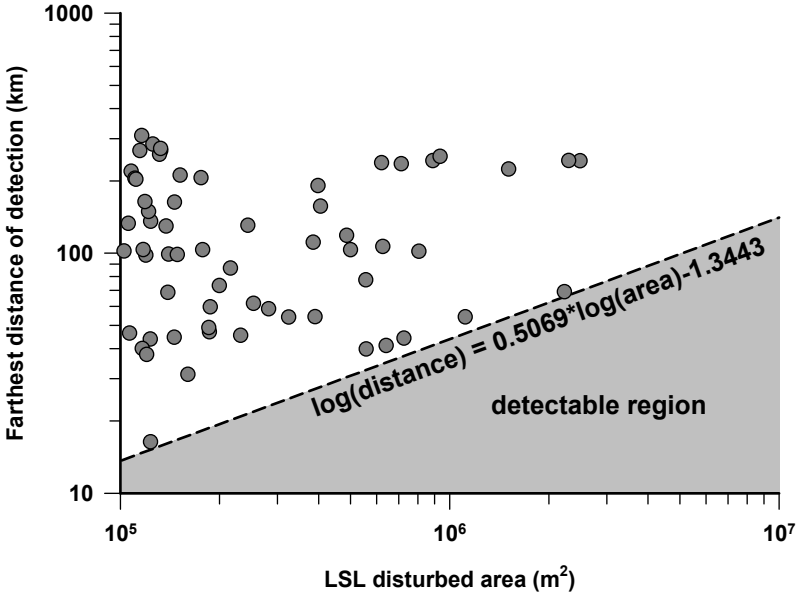

Fig. 9. Maximum distance of landslide-signal detection as a function of landslide-disturbed area. For a given LSL, the seismic signal should be visible at all stations plotted beneath the curve.